NASA TECHNICAL NOTE

NASA TN D-3751

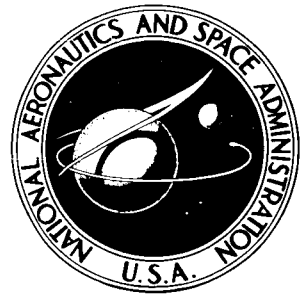

NASA TN D-3751

COLD-AIR INVESTIGATION OF A TURBINE FOR HIGH-TEMPERATURE-ENGINE APPLICATION

I. TURBINE DESIGN AND OVERALL STATOR PERFORMANCE

by Warren J. Whitney, Edward M. Szanca, Thomas P. Moffitt, and Daniel E. Monroe

Lewis Research Center
Cleveland, Ohio

NATIONAL AERONAUTICS AND SPACE ADMINISTRATION • WASHINGTON, D. C. • JANUARY 1967

NASA TN D-3751

COLD-AIR INVESTIGATION OF A TURBINE FOR HIGH-TEMPERATURE-ENGINE APPLICATION

I. TURBINE DESIGN AND OVERALL STATOR PERFORMANCE

By Warren J. Whitney, Edward M. Szanca,
Thomas P. Moffitt, and Daniel E. Monroe

Lewis Research Center
Cleveland, Ohio

NATIONAL AERONAUTICS AND SPACE ADMINISTRATION

For sale by the Clearinghouse for Federal Scientific and Technical Information
Springfield, Virginia 22151 – Price $1.00

COLD-AIR INVESTIGATION OF A TURBINE FOR HIGH-TEMPERATURE-ENGINE APPLICATION

I. TURBINE DESIGN AND OVERALL STATOR PERFORMANCE

by Warren J. Whitney, Edward M. Szanca,
Thomas P. Moffitt, and Daniel E. Monroe

Lewis Research Center

SUMMARY

A discussion of the design procedure for the single stage cold-air turbine is presented herein. The design velocity diagram and certain turbine geometric features were chosen to be typical of those of a turbine for high-temperature engine application. The characterizing features for this application are thick blade section, blunt leading and trailing edges, and low blade solidity.

The experimental investigation of the stator showed that the stator passed design equivalent weight flow at the design values of total- to static-pressure ratio which occurred simultaneously at the inner and outer walls. A comparison of the total- to static-pressure ratios across the stator at the inner and outer walls, with those calculated for free vortex outlet flow conditions, showed excellent agreement for pressure ratios up to incipient choking. The results of a survey of stator-outlet flow angle showed that the flow angle was close to the design value across the radial span and that this angle was only minutely affected by Mach number up to the stator choking point. The variation of the stator throat pressures with the overall pressure ratio indicated that choking occurred first at the hub section then progressed radially outward until the entire blade was choked. This behavior of throat pressures also indicated that, at supercritical pressure ratios, simple radial equilibrium is not maintained at the stator throat.

The blade-surface static-pressure measurements were used to compare the actual blade-surface velocity distribution with that evolved in the design procedure. This comparison shows that the design procedure gave a good indication of the trend and magnitude of the blade-surface velocities. The discrepancies noted between the actual and predicted surface velocities was felt to be attributable to the low blade solidity, whereas the stream-filament method used in the design procedure is especially suited to high solidity channels.

INTRODUCTION

In recent years, the advent of new types of aircraft such as the supersonic transport has stimulated renewed interest in higher engine-cycle temperatures. Studies such as reference 1, for example, have indicated the advantages of higher turbine-inlet temperature in terms of lower takeoff gross weight. This feature of increased turbine-inlet temperature dictates, in turn, that the turbine blading must be cooled in order to achieve its strength and operating-life requirements. The cooling methods generally considered for this turbine application utilize air bled from the compressor, directed through the blading, and ultimately discharged back into the main gas stream. The blade forms for this application are affected by the cooling requirements. The thickness must be increased to incorporate the internal coolant flow passages. In addition, the leading and trailing edges should be blunt so that adequate cooling can be applied to these critical areas. It is also desirable to employ high blade loading by using low solidity, thereby minimizing the amount of blade metal area. The blading design for this application is then compromised from what would be considered optimum (purely from an aerodynamic standpoint). Furthermore, it is desirable in some instances to have adjustable turbine-stator blades so that the engine can have more than one economical operational mode. Thus, the emergence of this new engine type has indicated the need for research to determine the effect on overall turbine performance of (1) the blading geometry that is compromised by cooling requirements, (2) the cooling air mixing with the main gas stream, and (3) the adjustable stators, as well as (4) the effect of a combination of these factors.

A considerable amount of research effort was devoted to this general field some years previous at NACA. Reference 2 presents a compilation of papers summarizing the results of much of this work. Currently, the interest in these advanced types of air-breathing propulsion engines has been renewed. The turbine research program at Lewis was accordingly expanded to include the turbine problem areas imposed by these engine types. The first-stage turbine of an advanced high-temperature engine for powering a supersonic aircraft was selected as typifing the problem areas. A 30-inch cold-air single-stage research turbine was designed with a velocity diagram and certain physical features that were characteristic of the selected turbine application. The turbine aerodynamic design was completed and the turbine stator assembly was fabricated. The stator assembly was installed in the test facility and investigated as a full annular cascade. In addition to the overall performance instrumentation, the stator blading was equipped with static-pressure taps at the hub, mean, and tip sections to obtain the surface pressure distribution.

This report presents the first phase of this program and includes the turbine design and the stator performance results. The surface pressure distributions are presented over a range of blade-outlet Mach number. At design Mach number, the blade-surface velocities are compared with those predicted by the design procedure.

SYMBOLS

A	area, ft^2
a	$-(\sin^2\beta/r)$
b	$2\omega \sin \beta$
c	blade chord, ft
g	acceleration due to gravity, 32.174 ft/sec^2
h	specific enthalpy, Btu/lb
J	mechanical equivalent of heat, 778.16 ft-lb/Btu
l	blade length, ft
n	orthogonal length, ft
o	throat dimension, ft
p	absolute pressure, lb/ft^2
R	gas constant, 53.34 ft-lb/(lb)(^oR)
r	radius, ft
s	pitch or blade spacing, ft
T	temperature, ^oR
U	blade velocity, ft/sec
V	absolute gas velocity, ft/sec
W	gas velocity relative to rotor blade, ft/sec
w	weight flow rate, lb/sec
α	absolute gas flow angle measured from axial direction, deg
β	relative gas flow angle measured from axial direction, deg
γ	ratio of specific heats
δ	ratio of inlet pressure to U.S. standard sea-level pressure, $p'_0/2116$
θ_{cr}	squared ratio of critical velocity at turbine inlet to critical velocity of U.S. standard sea-level air, $(V_{cr,0}/1019)^2$
ρ	gas density, lb/ft^3
ω	angular velocity, rad/sec

Subscripts:

ch channel

cr condition at Mach 1

d station downstream of turbine stator

h turbine hub section

i station at stator throat (see fig. 5)

m turbine mean section

t turbine tip section

u tangential component

x axial component

0 station at turbine inlet (see fig. 5)

1 station at stator-outlet free stream (see fig. 5)

2 station at rotor-outlet free stream

Superscript:

' total state condition

TURBINE DESIGN

The design requirements for the research turbine, selected to typify those of the first-stage turbine of an advanced high-temperature engine, are summarized as follows:

Equivalent specific work output, $\Delta h/\theta_{cr}$, Btu/lb	17
Equivalent mean blade speed, $U_m/\sqrt{\theta_{cr}}$, ft/sec	500
Design equivalent weight flow, $w\sqrt{\theta_{cr}}/\delta$, lb/sec	39.9
Tip diameter, in.	30
Hub diameter, in.	22
Stator outlet flow angle at mean radius, deg	67
Rotor outlet flow angle at mean radius, deg	-15 to -20

The 30-inch tip diameter selected was felt to be large enough to eliminate any detrimental Reynolds number effect on performance. The velocity diagram that was evolved to meet these requirements is shown in figure 1. All the quantities in the figure represent the free-stream uniform flow conditions into and out of the rotor. In order to obtain the total state conditions to construct the velocity diagram, it was necessary to employ overall loss assumptions for the blading. It was assumed that the stator had an overall loss equivalent to a total pressure ratio p_1'/p_0' of 0.97. In order to obtain the total state out of the rotor, an overall turbine efficiency (based on p_0'/p_2') of 0.885 was as-

	Hub	Mean	Tip
	ft/sec		
U	423.1	500.0	576.9
$V_{u,1}$	859.8	727.6	630.5
$V_{u,2}$	146.1	123.6	107.2
$V_{x,1}$	308.8	308.8	308.8
$V_{x,2}$	385.8	385.8	385.8
V_1	913.6	790.4	702.1
V_2	412.5	405.1	400.4
W_1	534.9	383.6	313.4
W_2	687.6	733.3	785.4

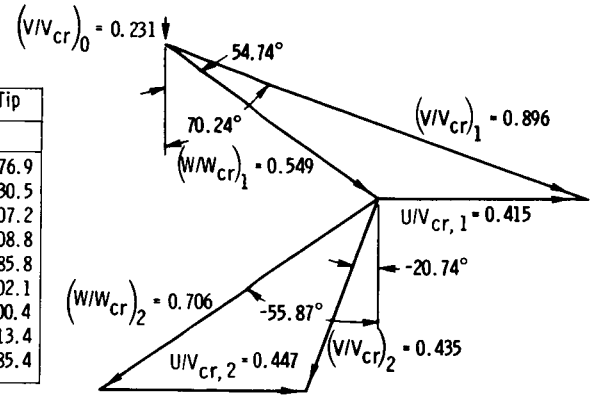

(a) Hub section; radius ratio, r/r_t, 0.733.

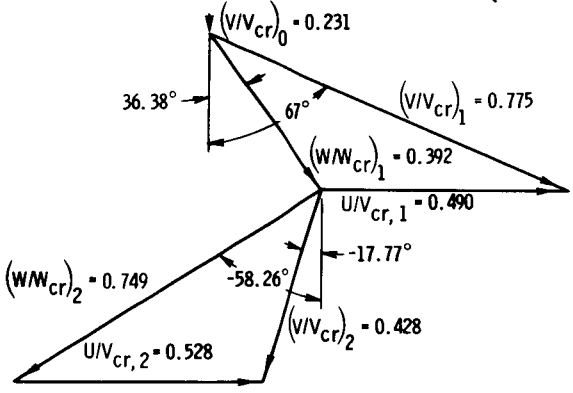

(b) Mean section; radius ratio, r/r_t, 0.8666.

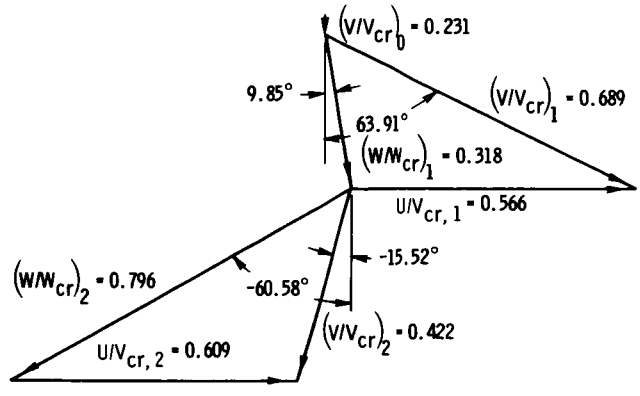

(c) Tip section; radius ratio, r/r_t, 1.000.

Figure 1. - Turbine design velocity diagram. All vector values in table refer to conditions at U.S. standard sea level air.

sumed. This efficiency assumption was based on the value of mean speed-work parameter $U_m^2/gJ\,\Delta h$ of 0.587, reference 3, and a small correction for Reynolds number. The corresponding turbine total-pressure ratio p'_0/p'_2 was 1.798.

The velocity diagram (fig. 1) indicates that this is a conservative design. The maximum rotor turning at the hub is 110.6°, and minimum reaction occurs at this section where the critical-velocity ratio W/W_{cr} increases from 0.549 to 0.706. The maximum critical-velocity ratios are $\left(V/V_{cr}\right)_1 = 0.896$ at the stator hub and $\left(W/W_{cr}\right)_2 = 0.796$ at the rotor tip.

Blade Physical Characteristics

In addition to the velocity diagram, it was also a prime purpose to evolve turbine geometry that was typical of a high-temperature-engine turbine. For this reason, certain physical characteristics of the blading such as leading-edge radius to blade chord ratio, trailing-edge radius to chord ratio, maximum thickness to chord ratio, and trailing-edge wedge angle were selected that were representative of those that might actually be encountered in this type of turbine application. The geometric characteristics of the blading are given in table I for the mean section.

TABLE I. - BLADE GEOMETRIC CHARACTERISTICS

Geometric characteristic	Rotor blade	Stator blade
Leading-edge-radius to chord ratio	0.065	0.066
Trailing-edge-radius to chord ratio	0.015	0.015
Maximum thickness to chord ratio	0.20	0.22
Blade chord dimension, in.	2.290	2.263
Solidity, c/s	1.71	1.385
Aspect ratio, ℓ/c	1.75	1.77

The solidity was selected purposely low by using reference 4 as a guide. The aspect ratio was purposely small resulting in blade cross sections that were relatively large compared with the tip diameter.

Blade Outlet Geometry

The function of the blade outlet is to direct the flow from the closed channel condition to blade-outlet free-stream (or velocity diagram) condition. The ensuing discussion refers to the stator blade; however, the procedure was the same for both the rotor- and stator-blade outlets. The layout of this transitional area was made as follows: A flat-back design was first constructed (fig. 2(a)) by using the selected values of blade spacing and trailing-edge thickness. The relations of continuity, constant angular momentum, and constant total state between stations i and 1 were utilized so that

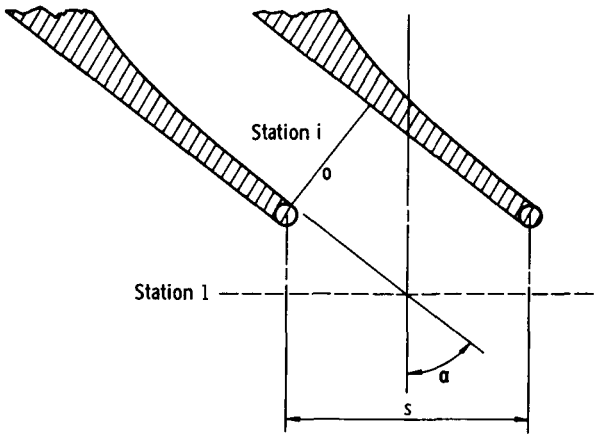

(a) Flat-back design.

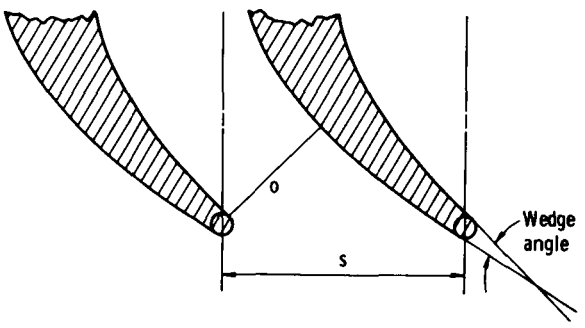

(b) Curved-back design.

Figure 2. - Sketch illustrating blade outlet design method.

$$V_{u,i} = V_{u,1}$$

$$(\rho V)_i o = (\rho V)_1 s \cos \alpha_1 \qquad (1)$$

where α_1 is the free-stream or velocity-diagram angle. The geometry was then adjusted, as in figure 2(b), by maintaining the same o dimension and by orienting the flow to a more axial direction at the throat orthogonal to obtain a thicker blade with a curved suction surface of constant curvature downstream of the throat. The stator- and rotor-blading-outlet sections were layed out in this manner to obtain a trailing-edge wedge angle (fig. 2(b)) of approximately 16°.

Blade Inlet Geometry

At the stator-blade inlet, the direction of the flow into the blading was axial, and no special design technique was applied to the layout of this section. The leading-edge circles were constructed and the blade thickness was increased quickly from the leading edge to obtain a thickened airfoil configuration.

The layout of the rotor-blade inlet was made by using the same procedure described for the outlets of the rotor and stator blading. The relations of continuity, constant angular momentum, and constant total state between the free stream relative condition and the first channel orthogonal position were applied as discussed for the blade outlets.

Blade Channel Design

The blade channels were layed out by using the following assumptions: (1) free vortex flow ahead of and downstream of the rotor, (2) simple radial equilibrium throughout, and (3) linear variation of the blade loss assigned to each blade row through the blade channel in proportion to the length of the mean flow path.

The blade-design method was similar to that described in reference 5 in that it was quasi-three-dimensional in nature consisting of sectional solutions at the hub, mean, and tip radii and an axisymmetric solution in the radial-axial plane. The hub, mean, and tip sections were layed out to achieve smooth surface-curvature variation and smooth area variation from the inlet to the outlet transitional part of the blade.

Orthogonal lines were sketched in the channel at many locations on each sectional layout and a midchannel streamline was drawn perpendicular to the orthogonals at their midpoints. At each of the orthogonal positions for each section, the following quantities were tabulated: suction surface curvature, pressure surface curvature, orthogonal length, midchannel flow angle, and length of mean flow path from blade inlet.

The ratio of surface velocity to midchannel velocity could then be obtained for any orthogonal by using the stream-filament method of reference 6 (or for any intermediate position between orthogonals by the use of appropriate cross plots).

The axisymmetric solution of the flow in the radial-axial plane was obtained by using the following equation, which is a form of equation (3) of reference 7

$$W = e^{\int_{r_m}^{r} a\,dr}\left(W_m - \int_{r_m}^{r} b\, e^{-\int_{r_m}^{r} a\,dr}\,dr\right) \tag{3}$$

where

$$a = -\frac{\sin^2\beta}{r}$$

$$b = 2\omega \sin\beta$$

This simplified form of the equation resulted from the assumptions of simple radial equilibrium and of zero curvature of the streamlines in the radial-axial plane. This equation yields the axisymmetric velocity at any radius, if the velocity at the mean radius and the radial variation of flow angle is known.

In the case of the stator blading, ω is zero and b is eliminated in equation (3). Also, for the stator blade, the relative-velocity terms and flow angles are the same as the absolute and are designated V and α. The procedure for applying this channel-design method was as follows:

(1) The blade surfaces and flow channels were constructed at the hub, mean, and tip sections, as discussed previously, and the sections were positioned in their actual rela-

tive axial locations.

(2) An arbitrary number of axial positions were chosen for the axisymmetric solution to define adequately the channel velocity distribution. The average flow angle β was taken as the midchannel streamline angle at the particular axial position.

(3) Equation (3) was then used to obtain the radial variation of velocity. A trial value of velocity was first assumed at the mean radius. The radial variation of midchannel flow angle was obtained by fitting a curve through the three known points at the hub, mean, and tip radii.

(4) The radial variation at velocity from step (3) was then used along with the section parameters to integrate the channel weight flow across the orthogonal surface

$$w_{ch} = \int_0^n \int_{r_h}^{r_t} \rho V \, dn \, dr \tag{4}$$

The velocity from the radial-axial solution (step (3)) was assumed to be the same as the section midchannel velocity. The integration across the orthogonals was performed at the

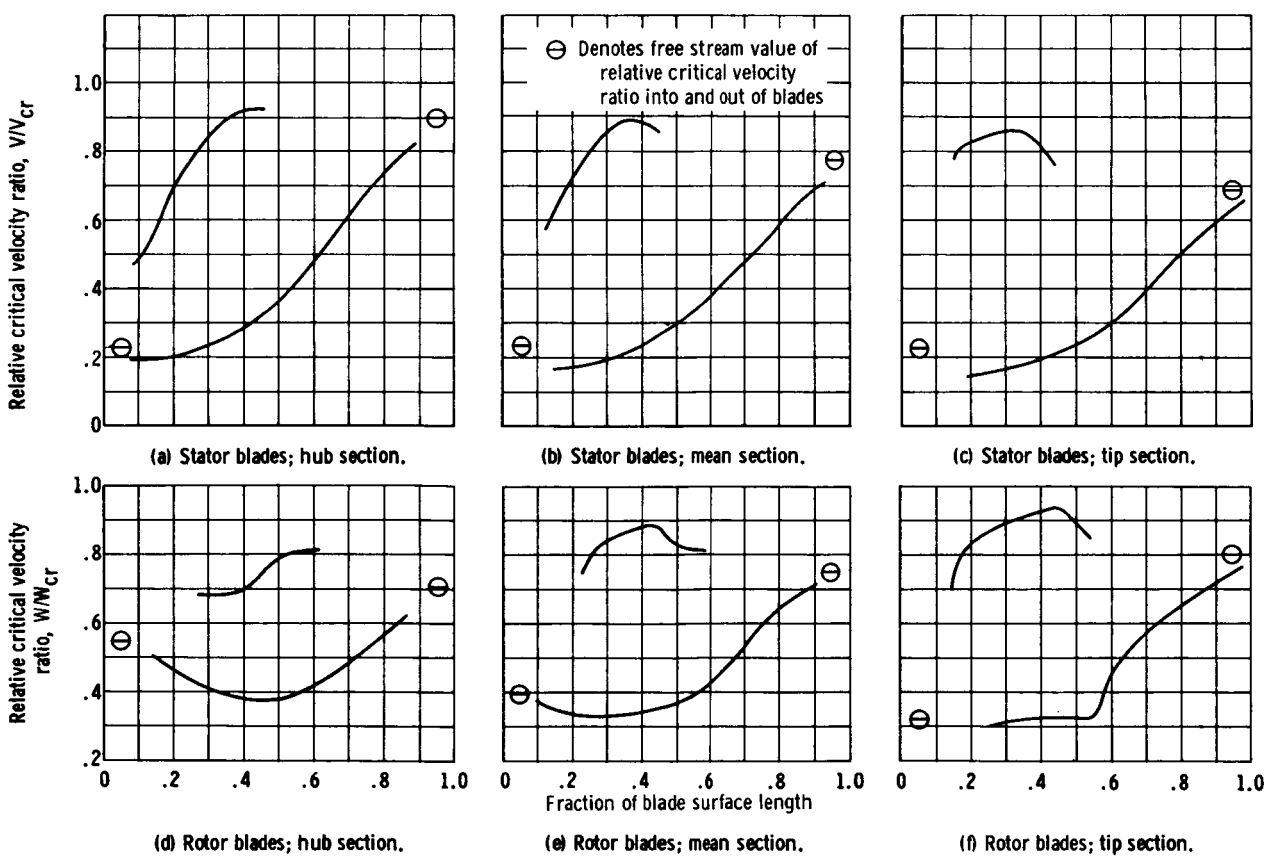

Figure 3. - Design blade-surface velocity distributions.

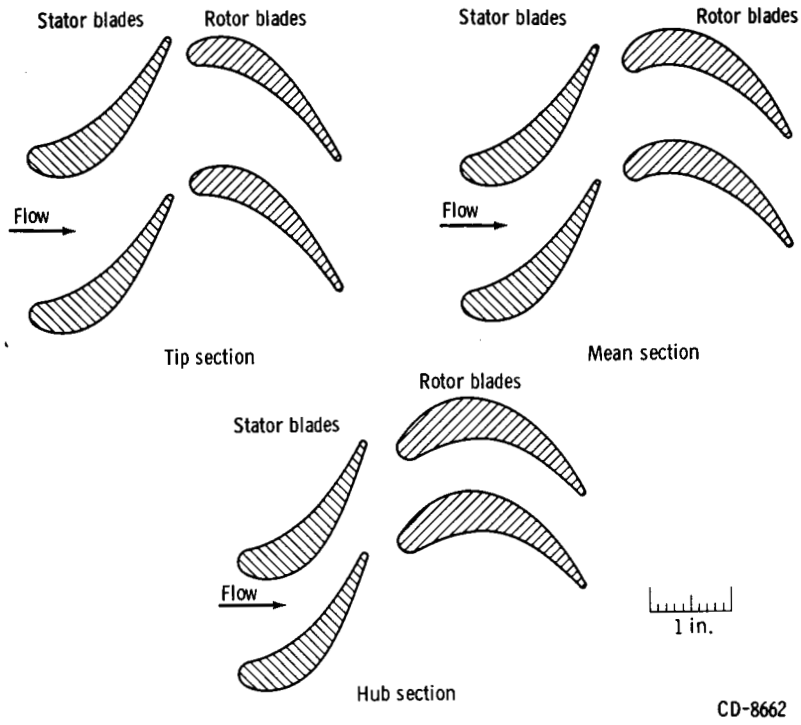

Figure 4. - Sketch of stator and rotor blade profiles and flow passages.

hub, mean, and tip sections by assuming that the blade-to-blade streamline curvature varied linearly across the orthogonal as in reference 6.

Equations (39) and (40) of reference 6 were used to obtain the surface velocities in terms of midchannel velocity. The radial integration was made by using Simpson's rule and the three known values of ρVn.

(5) If the integrated weight flow did not check the design value to 0.15 percent, a new estimate of mean radius velocity was entered in step (3) and the procedure was iterated until the weight flow was satisfied to this accuracy.

(6) After the channel velocity level was adjusted so that the design weight flow was satisfied, the surface velocities were plotted. It was desired to have smooth variation of velocity along the surface and to have the deceleration or diffusion within reasonable limits. If the surface velocity distribution was not satisfactory, the section blade-surface contours were altered (step (1)), and the procedure was repeated until satisfactory surface velocity distributions were obtained.

The blade-surface velocity distributions for the stator and rotor blading are presented in figure 3 where the high blade loading can be noted especially at the tip section. Figure 4 shows the blade passages and profiles for the hub, mean, and tip sections. The stator- and rotor-blade coordinates are given in table II.

TABLE II. - TURBINE BLADE COORDINATES

(a) Stator

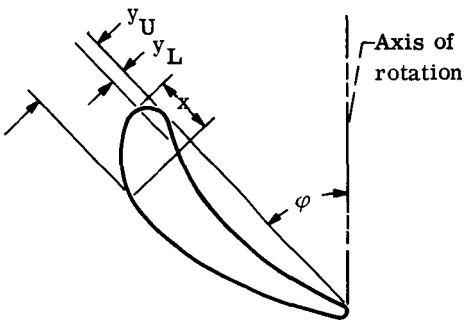

x, in.	Hub		Mean		Tip	
	Orientation angle, φ					
	42.42		41.03		39.67	
	Radius ratio, r/r_t					
	0.7333		0.8666		1.000	
	y_L, in.	y_U, in.	y_L, in.	y_U, in.	y_L, in.	y_U, in.
0	0.150	0.150	0.150	0.150	0.150	0.150
.100	-----	.375	-----	.394	-----	.427
.200	-----	.486	-----	.514	-----	.550
.300	.060	.558	.061	.588	.063	.621
.400	.105	.603	.106	.636	.111	.665
.500	.143	.630	.145	.665	.148	.688
.600	.174	.643	.174	.676	.179	.696
.700	.197	.643	.196	.675	.203	.690
.800	.214	.635	.210	.663	.217	.675
.900	.226	.618	.219	.644	.227	.651
1.000	.230	.595	.223	.619	.231	.625
1.100	.228	.570	.221	.590	.229	.597
1.200	.223	.541	.215	.560	.223	.565
1.300	.212	.508	.205	.527	.214	.535
1.400	.196	.473	.191	.492	.200	.500
1.500	.175	.433	.175	.452	.183	.462
1.600	.153	.391	.155	.410	.163	.422
1.700	.128	.345	.133	.365	.140	.380
1.800	.103	.295	.111	.319	.117	.335
1.900	.075	.242	.086	.267	.095	.287
2.000	.046	.183	.060	.214	.070	.237
2.100	.016	.121	.033	.157	.045	.185
2.197	.035	.035	-----	-----	-----	-----
2.200	-----	-----	.005	.096	.021	.130
2.263	-----	-----	.035	.035	-----	-----
2.327	-----	-----	-----	-----	.035	.035

TABLE II. - Concluded. TURBINE BLADE COORDINATES

(b) Rotor

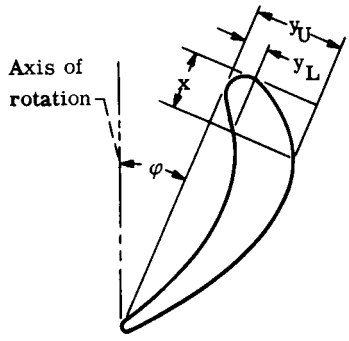

x, in.	Hub		Mean		Tip	
	Orientation angle, φ					
	11.31		22.87		34.67	
	Radius ratio, in.					
	0.7333		0.8666		1.000	
	y_L, in.	y_U, in.	y_L, in.	y_U, in.	y_L, in.	y_U, in.
0	0.150	0.150	0.150	0.150	0.150	0.150
.100	-----	.393	-----	.358	-----	.312
.200	-----	.536	-----	.490	-----	.397
.300	.075	.642	.078	.593	.066	.468
.400	.149	.725	.153	.668	.122	.523
.500	.219	.788	.217	.722	.168	.565
.600	.283	.839	.267	.755	.204	.593
.700	.338	.875	.307	.774	.232	.610
.800	.383	.900	.339	.781	.250	.614
.900	.416	.913	.360	.775	.262	.609
1.000	.439	.913	.373	.759	.264	.594
1.100	.453	.902	.377	.734	.261	.573
1.200	.458	.878	.373	.702	.252	.547
1.300	.454	.845	.362	.664	.237	.519
1.400	.442	.801	.342	.620	.220	.487
1.500	.422	.748	.315	.573	.200	.453
1.600	.393	.689	.283	.523	.177	.416
1.700	.356	.624	.244	.466	.153	.377
1.800	.312	.555	.203	.407	.128	.333
1.900	.260	.481	.159	.346	.103	.288
2.000	.202	.400	.113	.277	.077	.238
2.100	.140	.312	.067	.204	.050	.185
2.200	.072	.216	.022	.125	.022	.128
2.290	-----	-----	.035	.035	-----	-----
2.300	-----	.110	-----	-----	-----	-----
2.321	-----	-----	-----	-----	.035	.035
2.354	.035	.035	-----	-----	-----	-----
	Stacking axis coordinates					
	x = 1.200	y = 0.401	x = 1.110	y = 0.376	x = 1.080	y = 0.337

Blade Section Stacking Procedure

The stator blade was formed by stacking the three plane sections on a radial line that passed through the center of their trailing-edge circles and by fairing between the sections. The fairing lines were made to connect approximately equal percentages of the surface between the leading and trailing edges, and these lines were straight, or nearly so, in all cases. The stator assembly consisted of 50 blades. At the inner wall, the blades were secured by a round pin that protruded from the end of the blade. At the outer wall, the blade extended into a contoured hole that matched the airfoil shape.

The rotor blade was formed by stacking the three sections on a radial line and fairing in a manner similar to that described for the stator blade. The stacking axis, that was a radial line, was close to the centroids of the three sections, and the coordinates of the stacking axis are given in table II(b). The blade sections were positioned so that the relative displacement of the leading and trailing edges, as viewed in the sectional plane (perpendicular to the stacking axis), varied in proportion to the distance between the sections. The leading and trailing edges were straight and the fairing lines were very nearly straight. The rotor assembly consisted of 61 blades.

APPARATUS, INSTRUMENTATION, AND PROCEDURE

The test facility was designed to incorporate a complete research turbine and to provide low-temperature air for stator and rotor cooling. This phase of the investigation was concerned with evaluating the overall performance of the stator without cooling air.

Apparatus

The apparatus consisted of the design stator and test section together with suitable ducting and control valves. A diagramatic sketch of the stator test section is shown in figure 5 and a photograph of the test facility in figure 6. The stator was a full annular cascade of 50 hollow, cast, stainless-steel blades. The outer or tip diameter was 30 inches, and the inner or hub diameter was 22 inches. Figure 7 is a view of the stator installed in the test facility with the downstream ducting removed. Dry pressurized air was supplied from the combustion air system. A calibrated Dall tube, which is a special type of venturi meter, was located in a straight section of the inlet ducting for the purpose of measuring the weight flow. The turbine-inlet pressure was controlled by butterfly throttle valves located between the Dall tube and the inlet plenum chamber. After leaving the stator, the air was ducted to the altitude exhaust system through butterfly valves that were

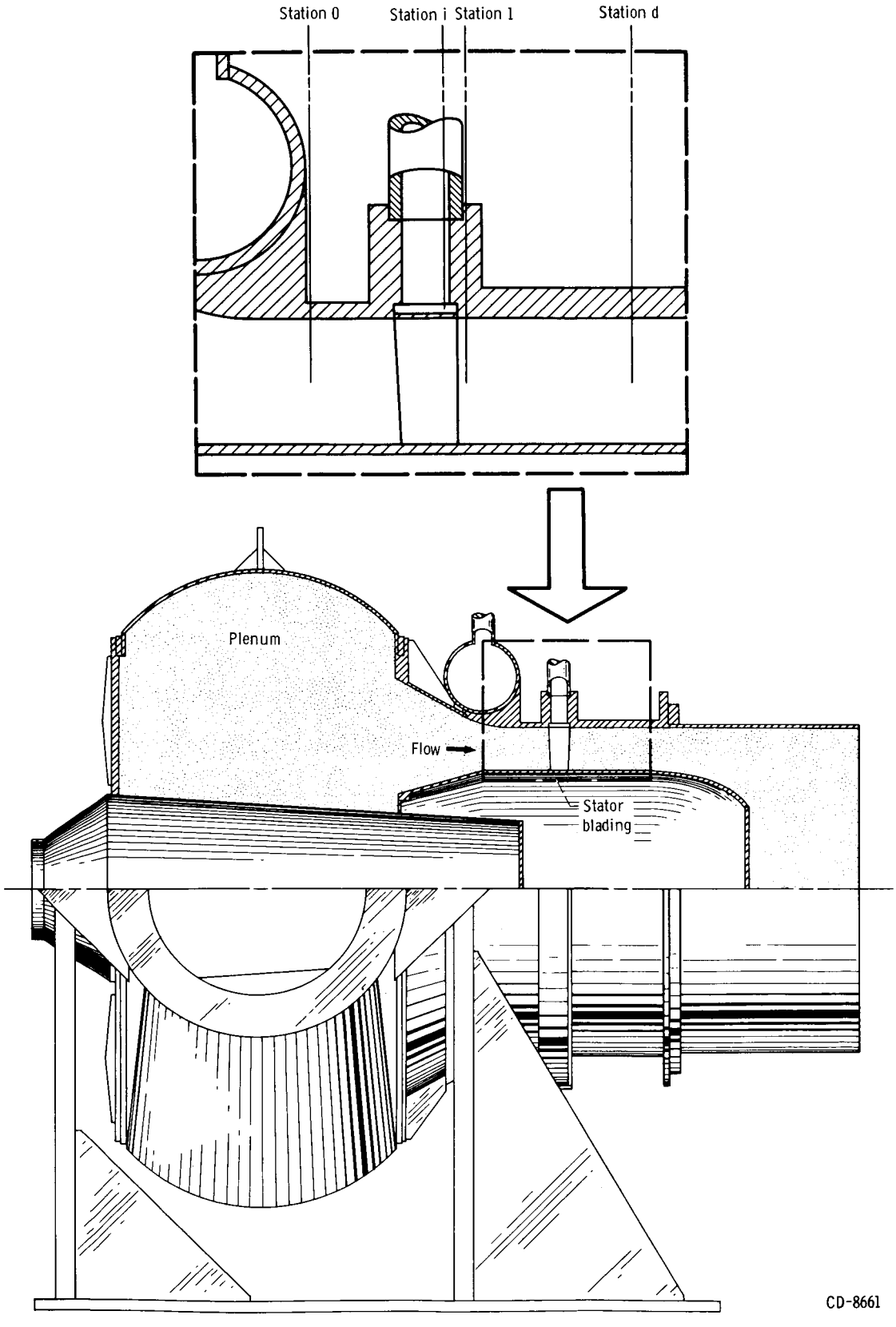

Figure 5. - Schematic diagram of turbine-stator test section.

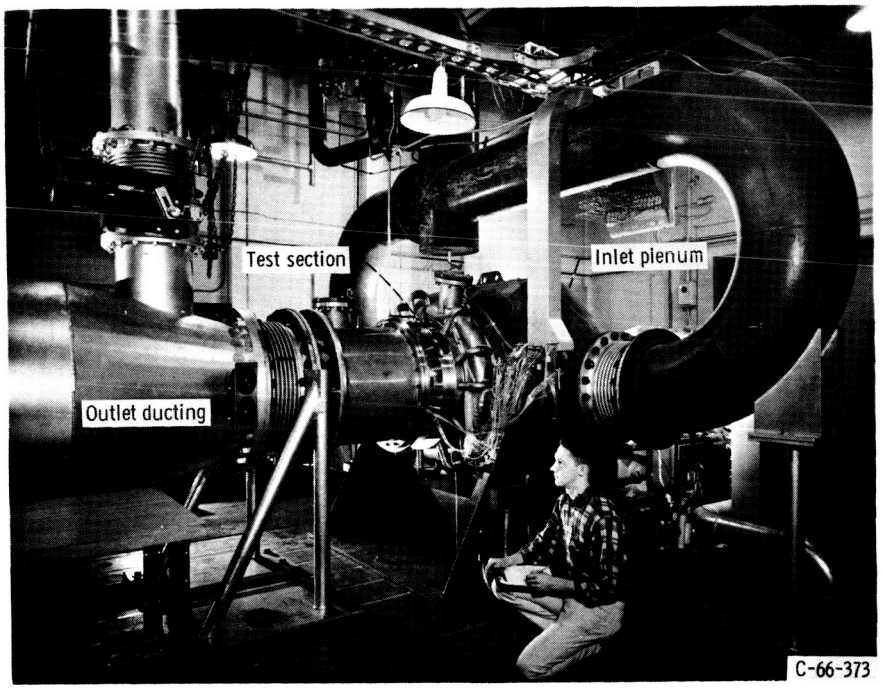

Figure 6. - Test facility.

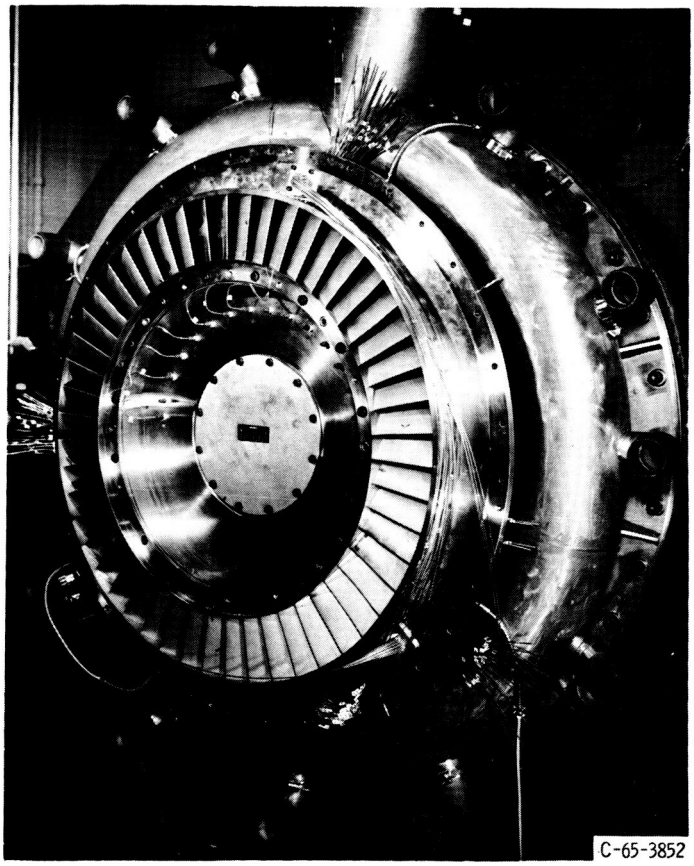

Figure 7. - Stator assembly installed in test facility.

used to control the outlet pressure.

Instrumentation

The turbine-stator test section was instrumented at four axial stations (fig. 5). At each of the stations were located eight static-pressure taps, four each at the inner and outer walls. The inner and outer taps were located opposite each other and were spaced 90° apart about the circumference, with the exception of station i. At this location, the taps were situated at the center of the throat orthogonals of four stator passages that were spaced 90° apart to the nearest passage.

At the inlet to the stator (station 0) four Kiel type total pressure probes were located at the area center radius and were spaced 90° apart circumferentially. Also, at this station, were located two thermocouple rakes, spaced 180° apart circumferentially, with each rake containing five thermocouples situated at the area center radii of five equal annular areas. Each group of four pressures, except those at the outlet (station d), were manifolded and connected to a single manometer tube. The eight outlet static pressures at station d were read on individual manometer tubes. A total of 86 static-pressure taps were installed on the blade surface at the hub, mean, and tip sections of three blade passages. The static-pressure taps at the hub and tip sections were located 0. 1 inch from the inner and outer walls to avoid the end-wall boundary layer. The mean-section pressure taps were located midway between the inner and outer walls. The location of the blade-surface pressure taps is shown in figure 8 for a typical blade section.

All pressures were read on mercury fluid manometers unless otherwise noted and all temperatures were read with a direct-reading self-balancing potentiometer.

The weight flow through the stator was measured with the Dall tube by using the stream temperature, Dall tube upstream pressure, and Dall tube differential pressure. The differential pressure was read on a tetrabromoethane fluid manometer. The flow angle at the stator outlet (station 1) was measured with a self-alining angle probe in conjunction with an X-Y plotter that recorded stator outlet angle as a function of radial position.

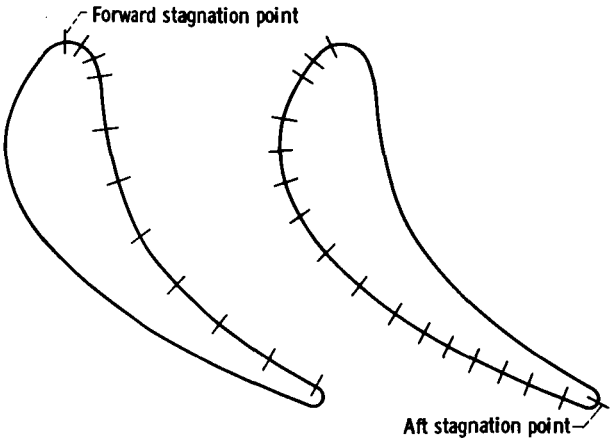

Figure 8. - Sketch of typical blade section showing location of blade-surface static pressure taps.

Procedure

The stator-inlet total-state conditions

were set and maintained at the nominal values of 30 inches of mercury absolute and 530° R. The overall pressure ratio $p_0'/p_{d,h}$ was obtained by setting the outlet pressure $p_{d,h}$ to the desired value. The weight-flow data were obtained over a range of overall pressure ratio by varying the outlet pressure. At each pressure ratio, the system was allowed to attain steady-state conditions, and the data were then recorded.

The static pressures along the blade surfaces were obtained at overall stator-pressure ratios corresponding to an approximate range of hub critical-velocity ratio $\left(V/V_{cr}\right)_{h,d}$ from 0.4 to 1.3. After the system had reached steady-state condition, the pressure readings of the hub, mean, and tip sections were recorded by photographing the manometer board. Weight-flow data were also recorded.

The flow-angle data were obtained at nominal hub critical-velocity ratios $\left(V/V_{cr}\right)_{h,d}$ of 0.5, 0.7, 0.896 (design), and 1.1 by traversing the angle probe radially across the blade span. The flow angle was measured at an axial position 1/2 inch downstream of the trailing edge with the sensing element of the probe situated in the flow path midway between two trailing edges. Overall stator performance in terms of pressure ratio, velocity distribution, pressure distribution, and weight flow were calculated.

The inlet total pressure used in this report was calculated from the average static pressure, inlet total temperature, annulus area, and weight flow from the following equation:

$$p_0' = p_0\left[\frac{1}{2} + \sqrt{\frac{1}{4} + \frac{\gamma - 1}{2g\gamma}\left(\frac{w}{p_0 A}\right)^2 RT_0'}\right]^{\gamma/(\gamma-1)} \tag{5}$$

RESULTS AND DISCUSSION

The experimental results include the overall stator performance results and the blade-surface pressure measurements. The overall performance is discussed first, and then the static-pressure distributions are presented. The static-pressure measurements at the design overall pressure ratio are used to compare the velocity distribution with that obtained in the design procedure.

Weight Flow

The experimentally obtained weight flows are shown in figure 9 over a range of stator pressure ratio at the inner and outer walls. Any given data point appears as two points

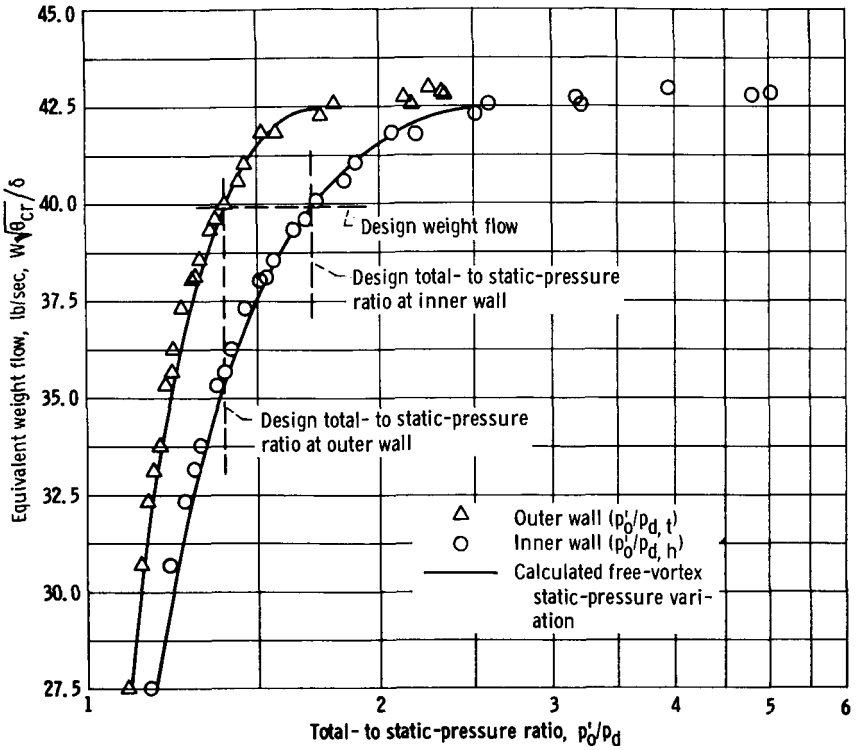

Figure 9. - Variation of equivalent weight flow with total- to static-pressure ratio at inner and outer walls.

in the figure, since, for a given weight flow, there is a resulting pressure ratio for the inner wall $p'_0/p_{d,h}$ and one for the outer wall $p'_0/p_{d,t}$. The design points shown in the figure represent design weight flow and design total- to static-pressure ratio at the inner and outer walls. Figure 9 indicates that the stator passed design equivalent weight flow (39.9 lb/sec) at the design values of pressure ratio at the inner and outer walls. As mentioned in the TURBINE DESIGN section, an overall loss pressure ratio p'_1/p'_0 of 0.97 was assumed, and the total pressure loss was assumed proportional to the length of the mean flow path. These assumptions correspond to a discharge coefficient at the stator throat of 0.98.

The solid lines in figure 9 represent a free vortex pressure distribution and they were generated as follows: The design-stator outlet angles were used to calculate free vortex outlet conditions for a range of pressure ratio up to the point where critical flow was obtained at the mean radius. A constant discharge coefficient was used that was equal to the design value. A total pressure loss was assumed that was proportional to the average kinetic energy level in the stator. The coefficient of this loss was evaluated to agree with the design loss pressure ratio of 0.97 at design flow conditions. A comparison of the lines with the experimental points in figure 9 indicates that, below choking, an approximate free vortex pressure distribution was obtained.

Thus, within the limits of experimental accuracy, it can be concluded that the stator passed design weight flow at design inner- and outer-wall pressure ratios, and that the stator closely approximated free vortex outlet conditions over a range of pressure ratios up to incipient choking.

Outlet Flow Angle

The stator-outlet flow angles are presented in figure 10 as a function of radial position for four values of the hub critical-velocity ratio. These angles were measured in a plane 1/2 inch axially downstream of the trailing edge with the probe situated in the center of the projected flow passage. They were felt to represent the free-stream or uniform-flow condition and, therefore, were comparable to the velocity-diagram angles. The solid lines in the figure are the actual angle traces recorded by the X-Y plotter. The wavy form of the trace results from the fact that the actuator drive would overcorrect the flow angle; the amplitude of this wave, however, is only about 1°. The dashed lines in the figure represent the design variation of flow angle with radius. Inspection of figure 10 indicates the greatest divergence from design flow angle (if the end wall effects are ignored) occurred about 1 inch from the inner wall. The overturning at this radius increased with increasing Mach number and amounted to about 2° at a hub critical-velocity ratio of 1.1. This trend may possibly be a result of a secondary flow core, which, in turn, would re-

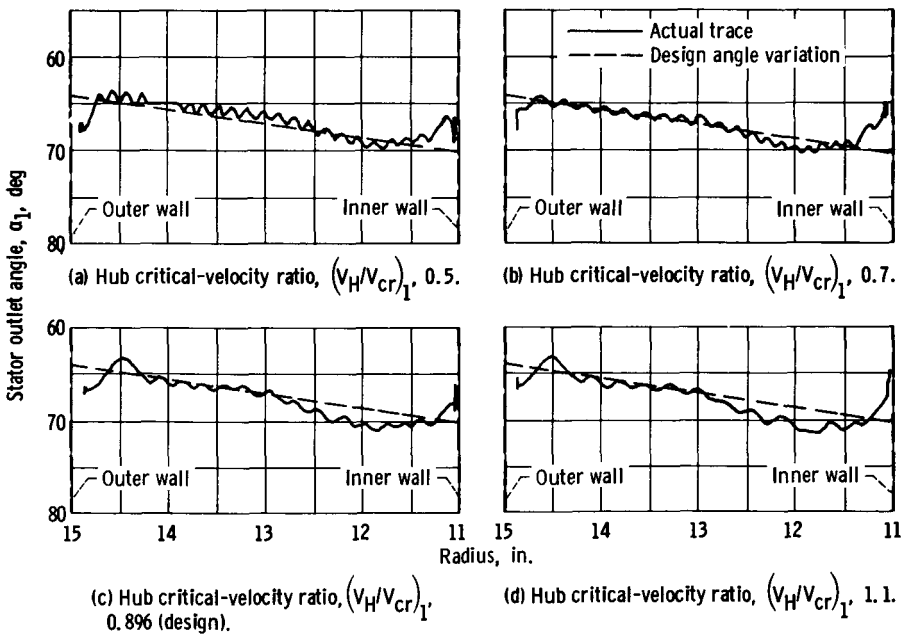

Figure 10. - Comparison of stator-outlet flow angles with design values for range of outlet critical velocity ratio.

sult in a circumferential total-pressure gradient. The pressure gradient would cause an error in the flow angle indication.

However, it can be concluded from the figure that, in general, the stator blade row performed its turning function well, in that the outlet angle distribution closely approximated design. It is also evident that the flow angle and angle distribution were only slightly affected by Mach number over the range of conditions covered in the investigation.

Throat-Pressure Ratios

As mentioned in the APPARATUS, INSTRUMENTATION, AND PROCEDURE section, throat pressures were measured at the inner and outer walls with four taps at each location situated at the midpoint of the throat orthogonal. The throat pressure ratios are shown in figure 11 as a function of an overall pressure ratio which is based on inlet total and the downstream inner-wall static pressure $p_0'/p_{d,h}$. The abscissa pressure ratio $p_0'/p_{d,h}$ is used merely to show the behavior of the throat pressures with overall pressure ratio. The outer-wall pressure ratio $p_0'/p_{d,t}$ could have been used as well; however, the inner-wall pressure ratio has a larger variation and provides a better spread of the data points.

The inner wall or hub value of throat pressure ratio increases with overall pressure ratio up to an overall value of about 2.6. At overall pressure ratios of 2.6 and greater, the hub throat pressure ratio holds nearly constant at a value of 1.99. The tip or outer-wall throat-pressure ratio starts to increase sharply at the overall pressure ratio of 2.6, attains the value of 1.99 at an overall pressure ratio of about 3, and remains constant for increasing values of overall pressure ratio.

The behavior of the throat pressures indicates that the stator row chokes progressively. The hub section starts to choke at an overall pressure ratio of 2.6, and the entire stator is choked at an overall pressure ratio of 3. These trends would indicate also that

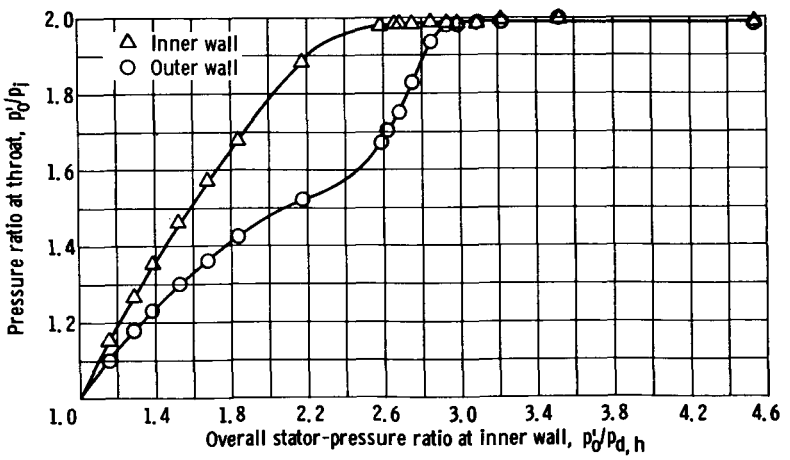

Figure 11. - Variation of stator throat pressure with overall stator-pressure ratio.

simple radial equilibrium is not maintained at the throat when the blade row is operated at supercritical pressure ratios. As mentioned, the choking pressure ratio was 1.99 for both the hub and tip throats. This value for a one-dimensional nozzle at choking conditions would be 1.89. At the choking orthogonal, where these pressures were measured, there is some curvature on both the suction and pressure surfaces. Thus, the measured pressure may not represent the average pressure for the throat.

Blade-Surface Pressure Distributions

The blade-surface pressure distributions are presented in figure 12 for the hub, mean, and tip sections for a range of hub critical-velocity ratio from 0.38 to 1.3. The ratio of surface static pressure to inlet total pressure is shown as a function of fraction of blade-surface length. The abscissa values of 0 and 1.0 correspond to the forward and aft stagnation points, respectively. The pressure decreases, generally, with increasing critical-velocity ratio. On the suction surfaces (figs. 12(b), (d), and (f)), a considerable amount of expansion occurs downstream of the closed channel at the higher critical-velocity ratios. Also, at the two highest critical-velocity ratios, the pressure curves become coincident (up to the throat station) at the hub section indicating that this section is choking. This tendency is also indicated at the mean section, while at the tip it is less pronounced. The throat positions, that are indicated on the curves, were taken as the ends of the throat orthogonals.

Blade-Surface Velocity Distribution

The blade-surface static pressures were used to develop the surface-velocity distribution by using the relation

$$\frac{V}{V_{cr}} = \left\{ \frac{\gamma + 1}{\gamma - 1} \left[1 - \left(\frac{p}{p_0'} \right)^{\gamma - 1/\gamma} \right] \right\}^{1/2} \tag{6}$$

for design, overall stator pressure-ratio conditions $\left(V/V_{cr}\right)_{h,d} = 0.796$. The use of equation (6) assumes that the flow in the free stream is isentropic.

The surface velocity distributions evolved in the design procedure (fig. 3, p. 9) were based on an overall total-pressure loss that varied in proportion to the length of flow path through the stator passage. Although this type of loss assumption is commonly used in design procedures, its use assumes that the boundary layer is instantly and intimately mixed with the free-stream flow causing a reduction in total pressure. A more comprehensive and correct technique would be to assume isentropic flow outside the boundary

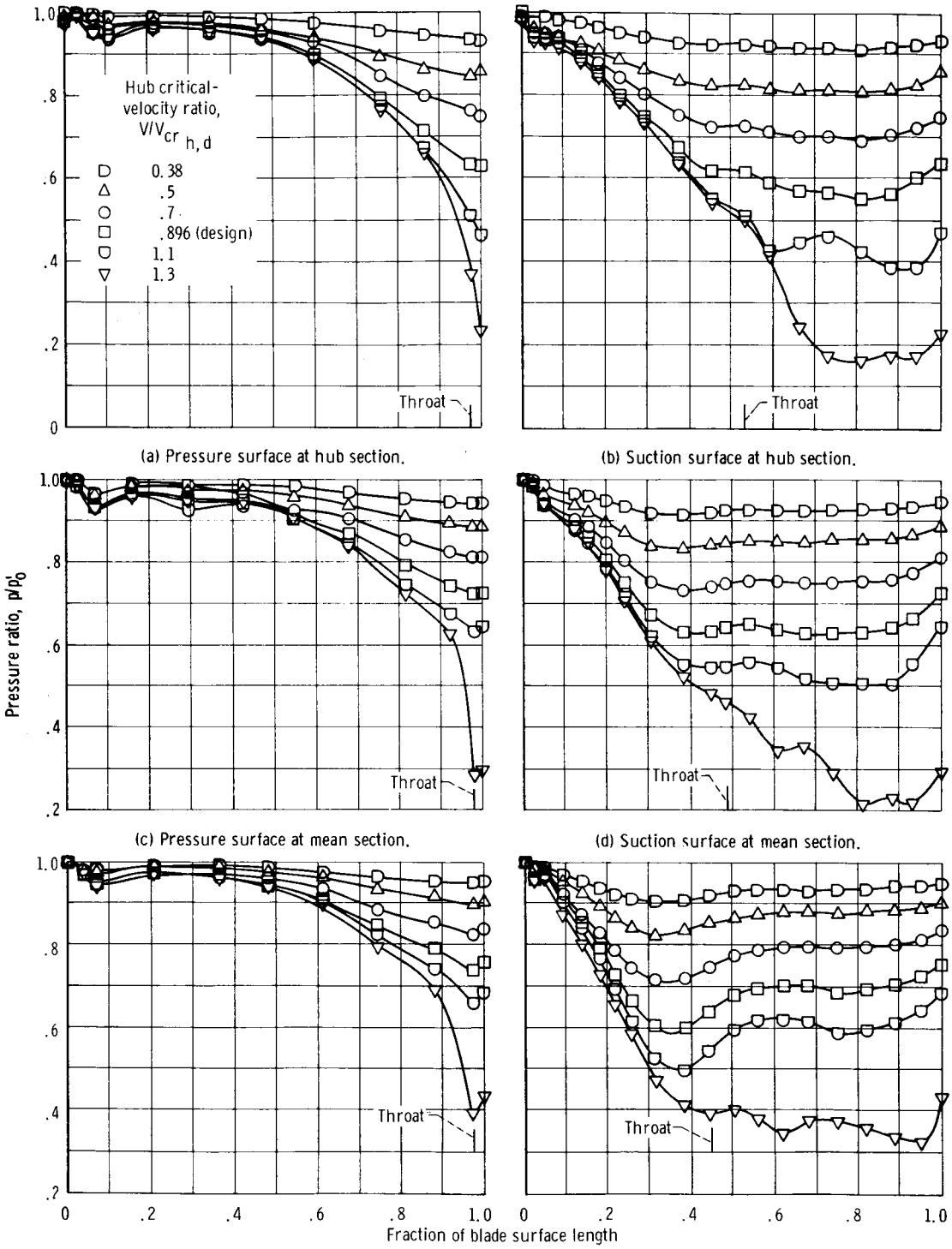

(a) Pressure surface at hub section.

(b) Suction surface at hub section.

(c) Pressure surface at mean section.

(d) Suction surface at mean section.

(e) Pressure surface at tip section.

(f) Suction surface at tip section.

Figure 12. - Blade-surface pressure distribution.

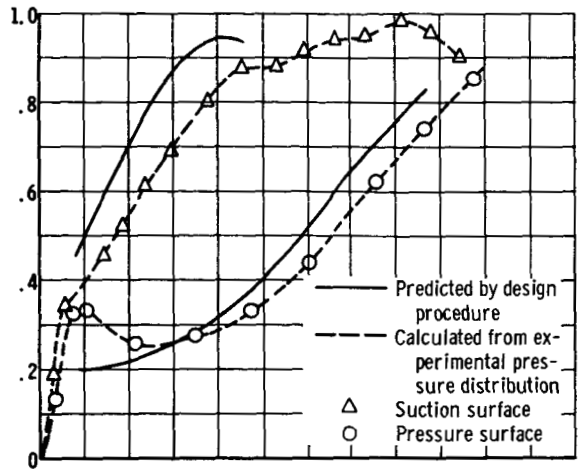

(a) Hub section.

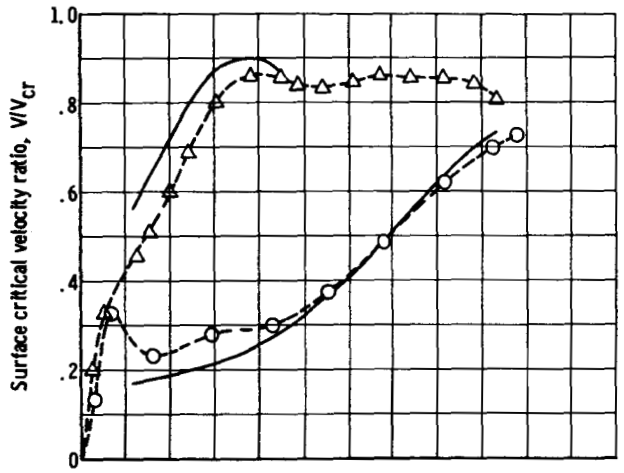

(b) Mean section.

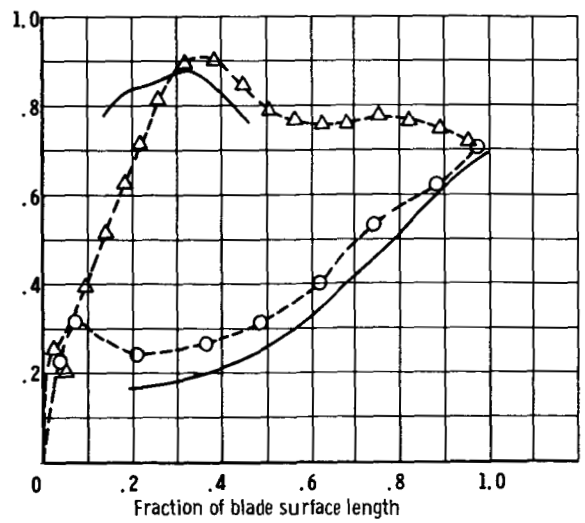

(c) Tip section.

Figure 13. - Comparison of design predicted surface velocity with experimentally obtained surface velocity at design pressure ratio.

layer with an area allowance for the boundary layer included to size the flow channel. Because the experimentally obtained velocity distributions were based on the assumption of isentropic free-stream flow, it was necessary to obtain a similarly based design velocity distribution to make them comparable. This was done for the comparison by factoring out the total-pressure loss that was used in the design procedure.

Figure 13 compares the experimental velocity distribution with the design distribution corrected for loss factor. The slight difference in design velocity from that of figure 3 (p. 9) is the result of eliminating the loss factor. The comparison (fig. 13) shows that the loading in the forward part of the blade (as indicated by the difference between suction- and pressure-surface velocities) is not as high as that predicted by the design procedure. The probable explanation for this difference is that, because of the low solidity, stream-filament theory (ref. 6) is less adaptable to this portion of the channel. This effect is also more pronounced at the tip section where solidity is lowest. Near the aft portion of the blade channel, the experimentally obtained velocities tend to be somewhat lower at the hub, somewhat higher at the tip, and about equal at the mean when compared with the design velocity distribution.

In general, it can be concluded that the design procedure predicted approximately the correct shape of the loading curves and nearly the correct peak velocities. It is felt that the procedure would yield more accurate results for a flow passage that has a higher solidity. Reference 6 indicates the method to be applicable to high solidity blading.

SUMMARY OF RESULTS

The stator component of a turbine, which was designed to study the problems associated with turbines for high-temperature-engine application, has been investigated experimentally. In addition to the overall performance characteristics, such as weight flow and outlet-flow angle, the blade-surface static-pressure distributions at the hub, mean, and tip sections were obtained. The pertinent results of the investigation are summarized as follows:

1. The stator passed design equivalent weight flow (39.9 lb/sec) at the design values of pressure ratio that occurred simultaneously at the inner and outer walls.

2. The measured stator outlet angle agreed closely with the design outlet angle across the radial span for a range of pressure ratio. The outlet angle was affected very little by outlet Mach number up to a choking pressure ratio.

3. The total- to static-pressure ratios across the stator at the inner and outer walls were in excellent agreement with the outlet pressure distribution calculated for free-vortex outlet-flow conditions for pressure ratios up to incipient choking.

4. The variation of the stator-throat pressures at the inner and outer walls with over-

all pressure ratio indicated that choking started at the hub and progressed radially outward until choking was reached at the tip. This variation indicates that, at supercritical pressure ratios, simple radial equilibrium is not maintained at the throat.

5. A comparison of the blade-surface velocities obtained experimentally with those evolved from the design procedure showed that the design procedure predicted fairly well the shape and magnitude of the blade-surface velocities. The discrepancies noted were felt to be the result of applying the stream-filament method (which is essentially suited to high-solidity blade passages) to a low-solidity blading design.

Lewis Research Center,
National Aeronautics and Space Administration,
Cleveland, Ohio, September 1, 1966,
720-03-01-35-22.

Author

REFERENCES

1. Dugan, J. F., Jr.; Koenig, R. W.; Whitlow, J. B., Jr.; and McAuliffe, T. B.: Power For the Mach 3 SST. Astronautics and Aeronautics, vol. 2, no. 9, Sept. 1964, pp. 44-51.

2. NACA Conference on Turbojet Engines For Supersonic Propulsion. A Compilation Of Technical Material Presented. Lewis Flight Propulsion Laboratory, Oct. 8-9, 1953.

3. Stewart, Warner L.: A Study of Axial-Flow Turbine Efficiency Characteristics in Terms of Velocity Diagram Parameters. Paper No. 61-WA-37, ASME, 1961.

4. Miser, James W.; Stewart, Warner L.; and Whitney, Warren J.: Analysis of Turbomachine Viscous Losses Affected by Changes in Blade Geometry. NACA RM E56F21, 1956.

5. Miser, James W.; and Stewart, Warner L,: Investigation of Two-Stage Air-Cooled Turbine Suitable For Flight Mach Number of 2. 5. II - Blade Design. NACA RM E56K06, 1957.

6. Huppert, M. C.; and MacGregor, Charles: Comparison Between Predicted and Observed Performance of Gas-Turbine Stator Blade Designed For Free-Vortex Flow. NACA TN 1810, 1949.

7. Stewart, Warner L.: Analytical Investigation of Flow Through High-Speed Mixed-Flow Turbine. NACA RM E51H06, 1951.

"The aeronautical and space activities of the United States shall be conducted so as to contribute . . . to the expansion of human knowledge of phenomena in the atmosphere and space. The Administration shall provide for the widest practicable and appropriate dissemination of information concerning its activities and the results thereof."

—NATIONAL AERONAUTICS AND SPACE ACT OF 1958

NASA SCIENTIFIC AND TECHNICAL PUBLICATIONS

TECHNICAL REPORTS: Scientific and technical information considered important, complete, and a lasting contribution to existing knowledge.

TECHNICAL NOTES: Information less broad in scope but nevertheless of importance as a contribution to existing knowledge.

TECHNICAL MEMORANDUMS: Information receiving limited distribution because of preliminary data, security classification, or other reasons.

CONTRACTOR REPORTS: Technical information generated in connection with a NASA contract or grant and released under NASA auspices.

TECHNICAL TRANSLATIONS: Information published in a foreign language considered to merit NASA distribution in English.

TECHNICAL REPRINTS: Information derived from NASA activities and initially published in the form of journal articles.

SPECIAL PUBLICATIONS: Information derived from or of value to NASA activities but not necessarily reporting the results of individual NASA-programmed scientific efforts. Publications include conference proceedings, monographs, data compilations, handbooks, sourcebooks, and special bibliographies.

Details on the availability of these publications may be obtained from:

SCIENTIFIC AND TECHNICAL INFORMATION DIVISION

NATIONAL AERONAUTICS AND SPACE ADMINISTRATION

Washington, D.C. 20546